Monte Carlo calculation of effective attenuation coefficients for various compensator materials

F. C. P. du Plessis[a] and C. A. Willemse
Medical Physics Department, Faculty of Health Sciences, University of the Free State, P.O. Box 339, Bloemfontein, 9300 South Africa

(Received 14 November 2002; revised 23 May 2003; accepted for publication 23 May 2003; published 25 August 2003)

Effective attenuation coefficients for 6, 8, and 15 MV photon beams were derived and studied for various compensator materials for square beams with side lengths of 0.5, 1.0, 2.0, 3.0, and 5.0 cm. Calculations were based on depth dose data in water obtained from EGS4 based DOSXYZ Monte Carlo simulations. Depth dose data were calculated using different compensator materials as attenuators of variable thickness. The absorbed dose varied exponentially as a function of absorber thickness at any depth in water on the beam axis for all materials. The effective attenuation coefficient data were compared with measurements for wax, aluminum and brass with values from the literature. Theoretical narrow beam linear attenuation coefficients were calculated and compared with the Monte Carlo data. The effective attenuation coefficient data for all materials were parametrized as functions of field size and depth in water. The effective attenuation coefficient was also parametrized as a function of atomic number. It was found that the effective attenuation coefficients calculated from the DOSXYZ data using a simple source model correspond to measured data for wax, aluminum and brass and published data for lead. © *2003 American Association of Physicists in Medicine.* [DOI: 10.1118/1.1591432]

Key words: Monte Carlo, effective attenuation, compensator, beamlet, IMRT

I. INTRODUCTION

In certain radiation treatment procedures it is necessary to compensate for missing tissues with the purpose of obtaining a uniform dose distribution at a certain depth in the patient.[1–3] The use of a compensator has skin sparing advantages over the use of bolus.[4] Beam modifiers, e.g., blocks and compensators influence the radiation dose at a certain reference point in a phantom.[5–7] This is mainly attributed to primary radiation attenuation and scatter alteration.[8,9] Electrons are also liberated from the beam filter and can contribute to the surface dose in a patient.[10] The scatter effect due to beam modifying filters is of the order of 6% of the transmitted primary dose for a 1 cm copper attenuator for 4 MV photon beams and becomes more prominent for large fields.[4,11] Others[12] have studied the broad beam attenuation coefficient for lead at photon energies from Co-60 to 25 MV and found that the measured attenuation coefficients vary by as much as 16% when compared to narrow beam data. Attenuator induced first order scatter was also studied by means of the analysis of the Klein–Nishina Compton cross section.[13] It is known that the effective attenuation coefficient for these beam filters and wedges vary as a complicated function of the measurement depth in the phantom, the x-ray beam field size, the thickness and material of the filter and the energy of the radiation beam.[14–18] Monte Carlo codes such as DOSXYZ[19] can be used to determine effective[20] attenuation coefficients (EACs) for narrow beams. This quantity depends on field size due to lateral electronic equilibrium that becomes important in narrow beam geometries.[20] Data presented by previous authors[21,22] are mostly from measurements and do not include a comprehensive number of materials typically used for compensator manufacturing. The use of compensators has also shifted towards a need for obtaining uniform dose distributions in complete target treatment. Advanced radiation treatment planning such as inverse treatment planning can be used with compensators for beam intensity modulation purposes or IMRT.

One way of modeling the compensator is by dividing the photon beam into a set of beamlets or beam elements and using their weights as a basis for compensator design.[23] The desired beam modulation is then obtained by determining the thickness of the attenuator corresponding to each beamlet using EACs. In this study the aim is to study the effect of field (beamlet) size, depth and material on the EAC using the DOSXYZ Monte Carlo code. Compensator materials, namely wax, copper, brass, lead, and aluminum were used over the energy range 6 MV to 15 MV. The coefficients were derived for small fields conforming to typical beamlet dimensions as used in beamlet based[24] treatment planning algorithms. Monte Carlo codes such as MCDOSE[24] perform dose calculations in a patient model by dividing a beam into a set of beamlets. The dose contribution from each beamlet is then weighted according to a precalculated intensity map obtained from an optimization algorithm. The desired beam intensity modulation in practice can then be obtained from the manipulation of the leaf settings of an MLC[25] or from the use of a compensator. Knowledge of the absorbed dose variation as a function of attenuator material, attenuator cross section area, attenuator thickness and its variation over depth in a water phantom is required for compensator manufacturing.

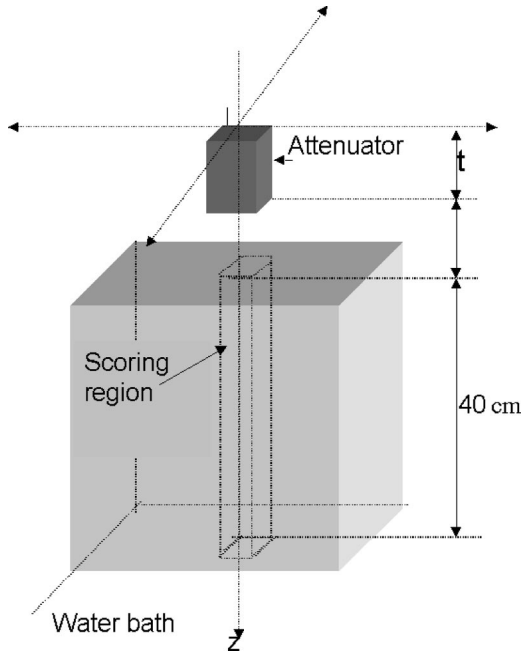

FIG. 1. The DOSXYZ geometry used for the determination of the effective attenuation coefficient for various attenuators. The beamlet area and thickness (t) of a block of compensator material were varied and the dose was scored in the scoring region consisting of voxels with x, y, and z dimensions of 0.5, 0.5, and 1 cm, respectively. Between the attenuator and the water phantom there was a 33 cm airgap. The dimensions of the water phantom were 40 cm in the x, y, and z directions.

II. METHODS

The EGS4[26] user code DOSXYZ was used to determine EACs for various attenuator materials by calculating the dose in a water phantom. Figure 1 shows the construction of the water phantom as well as the location of the attenuator. The attenuator and water phantom were incorporated into the same geometry. The dimensions of the water phantom were $40\times40\times40$ cm^3. The distance from the bottom of the attenuator to the top plane of the water phantom was 33 cm. The thickness (t) and the area of the attenuator were varied to coincide with beamlet dimensions. The attenuator materials that were used consisted of wax, copper, brass, lead, and aluminum. The x-ray source used was a parallel beam incident perpendicularly to the xy plane and its beam axis coincided with the z axis of the DOSXYZ coordinate system. Input energy spectra corresponding to 6, 8, and 15 MV x-ray sources were used. These spectra were obtained from BEAM[27] simulations for a Philips SL75/5 (6 MV), a Philips SL75/14N (8 MV), and a Philips SL25 (15 MV) accelerator. The energy spectra were obtained using the BEAMDP[28] code. The scoring planes were located just above the jaws for each accelerator. The depth dose was scored in a column of voxels, centered on the z axis of the phantom, with dimensions of $0.5\times0.5\times1.0$ cm^3 in the x, y, and z directions, respectively. This column extended to 40 cm in depth.

The DOSXYZ simulations were performed for a range of thickness of 0, 1, 2, 3, 4, 5, 6, 8, 10, 15, 20, 30, 40, and 50 mm for each compensator material except wax that was extended to 150 mm. These simulations were repeated for a range of beamlet areas consisting of squares with side lengths of 0.5, 1.0, 2.0, 3.0, and 5 cm. The depth dose data were analyzed by plotting it as a function of compensator thickness for different beamlet sizes. The number of histories chosen was enough to reduce the dose variance below one percent and is a function of the thickness of the compensator media and the voxel size. A thickness of 4 cm of copper required, for example, 10^8 histories.

Each of the MC generated depth dose curves were normalized to its own maximum dose. A FORTRAN code was written to fit a five parameter double exponential function to these normalized depth dose data from a depth of 4 cm down to 40 cm. The equation is of the form

$$\bar{D}_{\mathrm{med}}(z,A)=\alpha+\beta\exp(-\gamma z)+\delta\exp(-\varepsilon z), \tag{1}$$

where the five parameters, indicated by greek symbols (α–ε), were determined by a least square minimization method by iteratively choosing the fitted constants randomly to obtain the best fit between the MC calculated depth doses and the values calculated from Eq. (1). The fitted values agreed on average better than 1% locally with the MC generated dose values. From Eq. (1), $\bar{D}_{\mathrm{med}}$ indicates the normalized absorbed dose, at depth z, in water as a result of transmitted, scattered and in-phantom scattered x rays from absorber material, med, for a beamlet size A. The depth dose data were represented by these exponential functions to reduce the statistical variance below the one percent level. Some of the representative fitting constants are given in Table I. The calculated normalized depth dose data were multiplied by their respective normalization doses to obtain the smoothed absorbed dose data.

EACs were derived by plotting the logarithm of the smoothed depth dose values, for a given compensator material, beam energy and depth as a function of beam absorber thickness. A linear regression was performed on this data and the gradient of each fitted line was determined. This yielded

TABLE I. Representative values of the fitting constants that were derived by using Eq. (1). The left-most column indicates the material and in parentheses the beam energy, E (MeV), side length of square beamlet size, A (cm), and material thickness, t (cm).

Material (E,A,t)	α	β	γ (cm^{-1})	δ	ε (cm^{-1})
Wax (8,5,8.0)	1.3386	0.0572	−0.2963	0.0816	0.0594
Lead (15,3,3.0)	1.5285	0.0467	−0.4873	0.0800	0.0953
Brass (8,5,1.0)	2.1919	0.0582	−1.1126	0.0765	0.0462
Al (8,2,1.0)	1.6985	0.0382	−0.7632	0.0183	0.1398
Cu (6,5,5.0)	1.3455	0.0381	−0.3124	0.0130	0.1146

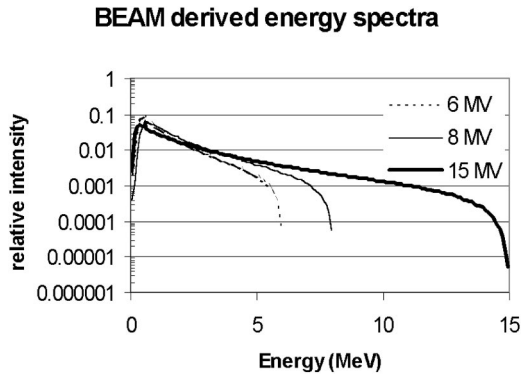

FIG. 2. The energy spectra derived from the BEAM MC code simulations for the Philips SL75/5 (6 MV), Philips SL75/14N (8 MV) and Philips SL25 (15 MV) accelerators. The area under each spectrum is normalized to unity.

the EAC. This can be seen by expressing the absorbed dose at a certain depth in the water phantom as

$$D_{\mathrm{med}}(z,A,t)=D_{\mathrm{med}}(z,A,t=0)\exp(-\mu_{\mathrm{eff}}t), \tag{2}$$

where t, d, A, and μ_{eff} represent thickness, depth, beamlet area, and EAC, respectively. $D_{\mathrm{med}}(z,A,t=0)$ indicates the dose in water for zero absorber thickness which thus corresponds to the depth dose for an open beamlet of size, A, at depth, z, in water.

The EACs for parrafin wax, aluminum and brass were also calculated from transmission measurements on the linacs on which the beam sources were based for a 3 $\times$3 cm field at an SSD of 100 cm and an airgap of 33 cm. The EAC were determined at an effective depth of 4 cm in a solid water phantom using a Farmer type 2571 graphite ionization chamber and a PTW UNIDOS electrometer.

III. RESULTS

Figure 2 shows the photon energy spectra used in this study for 6, 8, and 15 MV x rays, respectively.

The EAC for square beamlet areas with side lengths of 0.5, 1.0, 2.0, 3.0, and 5.0 cm are shown in Fig. 3 for brass as a function of depth in water. From these plots the EAC values decrease with depth. The change is of the order of 13% over a depth range from 4 cm to 39 cm for brass. The EAC

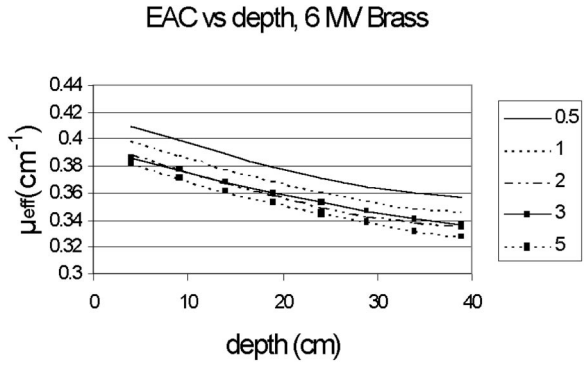

FIG. 3. The effective attenuation coefficient (μ_{eff}) as a function of depth in water for square beamlet areas with side lengths of 0.5, 1.0, 2.0, 3.0, and 5.0 cm.

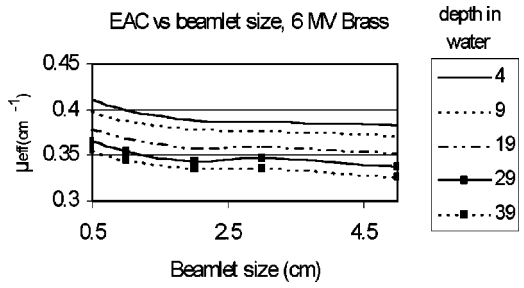

FIG. 4. Effective attenuation coefficients as a function of beamlet area at five constant depths of 4, 9, 19, 29, and 39 cm obtained for brass beam absorbers.

is largest for the smallest beamlet area of 0.5 cm side length and their values decrease progressively for larger beamlet sizes. This is due to more in-phantom scattered radiation for larger beamlet areas contributing to the dose in the central scoring region (see Fig. 1). The lack of lateral electronic equilibrium also enlarges these coefficients for the smaller beamlets[20] since more electrons scatter out of the scoring region than entering it as in the case of larger fields.

A set of plots of the variation of the EAC as a function of beamlet size at various depths is shown in Fig. 4 for brass. The variation of the EAC with energy (6, 8, and 15 MV) and field size (0.5, 3.0, and 5.0 cm) is shown in Fig. 5. The effective attenuation curves have the highest values for 6 MV beam energies (solid marked lines), followed by the values for 8 MV (broken lines) and 15 MV (solid lines without marks).

A. Effect of material type

In Figs. 6(a)–6(c) the dependence of the EAC for various materials for three beamlet areas of 0.5 cm, 1.0 cm, and 5.0 cm are shown for a 6 MV x-ray beam. Table II shows the atomic number values for the materials used in this study and a graph of the dependence of the EAC on atomic number (Z) is shown in Fig. 7. The EAC values for a 5×5 cm^2 beamlet at an energy of 6 MV could be parametrized by the equation

$$\mu_{\mathrm{eff}}=-0.0001Z^2+0.0169Z-0.0619, \tag{3}$$

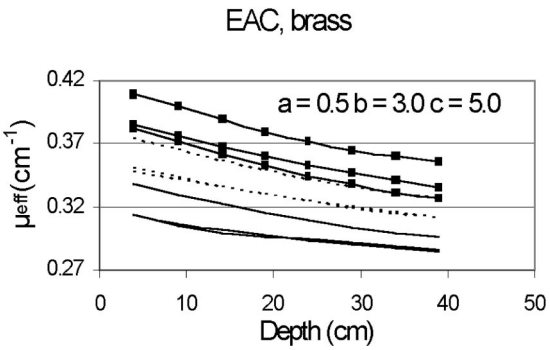

FIG. 5. Effective attenuation coefficients for brass as a function of depth for different beam energies (—■—, 6 MV; ---, 8 MV; and—, 15 MV). Each set of lines corresponds to three different beamlet sizes for the same energy. The smallest beamlet at a given energy has the larger effective attenuation value. Beamlet sizes correspond to 0.5, 3.0, and 5.0 cm side lengths.

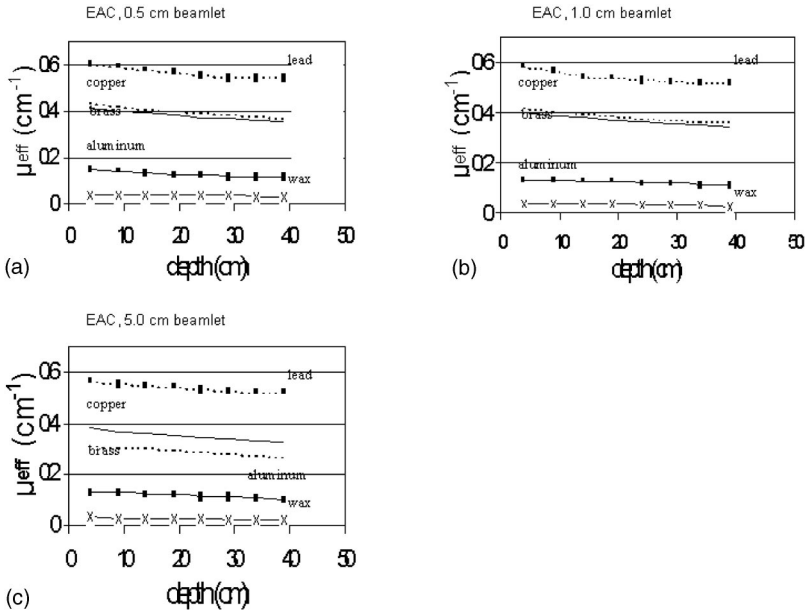

FIG. 6. The dependence of the effective attenuation coefficient on depth for various materials for beamlet areas of 0.5 cm (a), 1.0 cm (b), and 5.0 cm (c) are shown for a 6 MV x-ray beam.

where Z is the atomic number as found in column 3 in Table II. There exists a simple quadratic relationship between the atomic number of a material and its effective attenuation coefficient. The correlation between the data points and the fitted curve was better than 0.98.

Table III shows the EAC values for different materials as a function of field size. These EAC values were taken at a depth of 4 cm in water. The second column displays the values for the narrow beam attenuation coefficient as calculated with data from Hubbell and Seltzer.[29] These EAC values were calculated by using the spectra data in Fig. 1. The spectra were rebinned into 1 MeV bins and the corresponding narrow beam linear attenuation coefficients were calculated by weighing the energy related coefficients against the number of photons in the corresponding energy bins. From the table it can be observed that the calculated values correspond the EAC values for the 0.5×0.5 cm^2 beamlet for copper, brass and aluminum. Larger deviations occurred for wax and lead where the correspondence broke down.

B. Effect of depth and beamlet size

The EAC depend on depth in water as well as beamlet size as shown in Figs. 3 and 4 for brass. The dependence of the EAC with depth and field size can be parametrized by the equation

TABLE II. Materials used as beam absorbers in this study for the determination of their effective attenuation coefficients along with their physical densities. The mass electron density is expressed by Z/A.

Material	Density (g/cm^3)	Z	Z/A	Composition (wt. %)
Wax (dental)	0.90	5.7[a]	0.743	C:H:O (83:13:4)
Aluminum	2.69	13	0.482	Al (100)
Brass	8.47	29.3[a]	0.457	Zn:Cu (34:66)
Copper	8.93	29	0.456	Cu (100)
Lead	11.34	82	0.397	Pb (100)

[a]Effective atomic number calculated for Z^2 dependence of cross section.

$$\mu_{\text{eff}}=\mu_0(1-\mu_1 S^{1/3})-\mu_2 d, \tag{4}$$

where μ_0 is the theoretical narrow beam attenuation coefficient (see column 2 in Table III) and μ_1 indicates the effect of the square field size (S) and is related to the scatter contribution for the field size to the value of the EAC. The constant μ_2 indicates the decrease in the EAC as a function of depth. This parametrization could reproduce the EAC values within 1–3 % in most cases. In Table IV a summary of these coefficients is shown for the materials used in this study.

Figures 8(a) and 8(b) show how these coefficients vary as a function of depth for (a) varying retracting distances for 6 MV x rays and (b) various beam energies at a retracting distance of 10 cm. Both figures are reported for brass for a beamlet size of 5 cm.

A comparison between the Monte Carlo derived data and experimentally obtained data for paraffin wax, aluminum, and brass is shown in Table V. Data for lead as found in the literature are also included in the table.

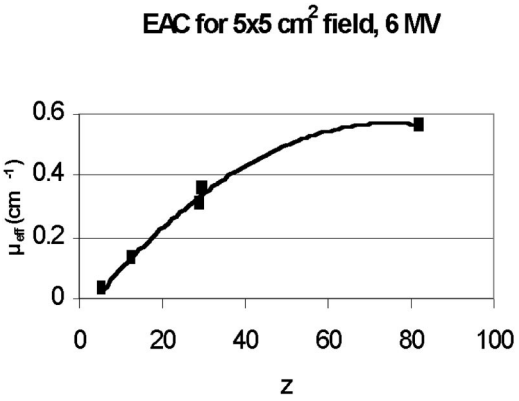

FIG. 7. The dependence of the EAC on the atomic number (Z) of the absorber material for a beam energy of 6 MV at a depth of 4 cm. The solid curve represents the fitting equation.

TABLE III. Effective attenuation coefficients (EAC) in units of cm^{-1} at a depth of 4 cm in water. This data is shown for various beamlet sizes and beam energies. The second column shows theoretically calculated EAC values based on the spectra in Fig. 1 and on narrow beam attenuation data.

6 MV beam energy	EAC (calculated)	Side length of square beamlet size (cm)				
Material	Narrow beam	0.5	1.0	2.0	3.0	5.0
Wax	0.052	0.039	0.039	0.038	0.037	0.037
Aluminum	0.147	0.144	0.134	0.132	0.131	0.131
Brass	0.411	0.410	0.400	0.389	0.386	0.382
Copper	0.438	0.431	0.417	0.368	0.314	0.311
Lead	0.659	0.605	0.578	0.573	0.571	0.564
8 MV beam energy	EAC (calculated)	Side length of square beamlet size (cm)				
Material	Narrow beam	0.5	1.0	2.0	3.0	5.0
Wax	0.047	0.037	0.035	0.034	0.034	0.031
Aluminum	0.129	0.126	0.119	0.115	0.115	0.114
Brass	0.373	0.375	0.359	0.351	0.350	0.350
Copper	0.407	0.394	0.371	0.368	0.367	0.367
Lead	0.607	0.564	0.548	0.541	0.537	0.537
15 MV beam energy	EAC (calculated)	Side length of square beamlet size (cm)				
Material	Narrow beam	0.5	1.0	2.0	3.0	5.0
Wax	0.045	0.037	0.037	0.028	0.028	0.023
Aluminum	0.122	0.110	0.103	0.098	0.098	0.096
Brass	0.371	0.339	0.327	0.316	0.313	0.313
Copper	0.395	0.355	0.338	0.324	0.329	0.325
Lead	0.615	0.545	0.537	0.530	0.527	0.527

IV. DISCUSSION

In Fig. 3 the EAC for brass decrease due to increased phantom scatter with depth. In Fig. 4 these coefficients are plotted as a function of depth in water for a set of beamlet sizes. These coefficients decrease with depth but the effect is relatively small. The range of variation of the coefficients is of the order of 14% over the depth range from 4 to 40 cm as seen from inspection of the data in Fig. 3 for a particular beamlet size. In Table III the EAC values for the materials studied are shown. The deviation of the calculated narrow beam EAC data shown in column 2 in Table III for wax and lead can be explained as follows: From Table II wax contains 13% hydrogen by weight that contributes to its relatively high electron density (Z/A) that is about 1.5 times higher compared to the other materials. The energy spectra were binned into 1 MeV intervals with all photons less than 1 MeV taken to have an energy of 1 MeV. About 50% of the photons lie in this bin and it was assumed that they have exactly this energy value. At 1 MeV the mass attenuation coefficient for hydrogen is about twice as high as that of other materials. This artificially enhances the value of the calculated EAC. In reality the attenuation of the lower energy components in wax will not be as severe as depicted by the EAC calculation. The electron density of lead is lower than that of Al, brass and copper, but its atomic number is much higher thus enhancing pair production. The rebinning process also introduced artificially high calculated EAC values. It is believed that a refinement of this calculation method would lead to more realistic narrow beam EAC values.

From Fig. 4 it can be observed that these curves obtained at depths of 4 and 9 cm tend to have a constant (almost horizontal) slope as the beamlet size further increases, indicating charged particle equilibrium that has been reached. The variation of these curves at different depths is of the same order as the statistical variance of the data. It can be shown from the use of Eq. (2) that the absolute change in the effective attenuation coefficient as a function of the percent-

TABLE IV. Fitting constants for the parametrization of the EAC for the materials used in this study.

Material	Energy (MV)	μ_0 (cm^{-1})	μ_1 $(cm^{-4/3})$	μ_2 (cm^{-2})
Wax	6	0.052	0.173	0.000 25
	8	0.047	0.233	0.000 24
	15	0.045	0.362	0.000 27
Aluminum	6	0.147	0.052	0.000 74
	8	0.129	0.037	0.000 56
	15	0.122	0.035	0.000 53
Brass	6	0.411	0.105	0.000 91
	8	0.373	0.020	0.001 20
	15	0.371	0.005	0.001 54
Copper	6	0.438	0.110	0.00156
	8	0.407	0.055	0.001 22
	15	0.395	0.121	0.000 97
Lead	6	0.659	0.088	0.000 16
	8	0.607	0.045	0.000 86
	15	0.615	0.105	0.000 51

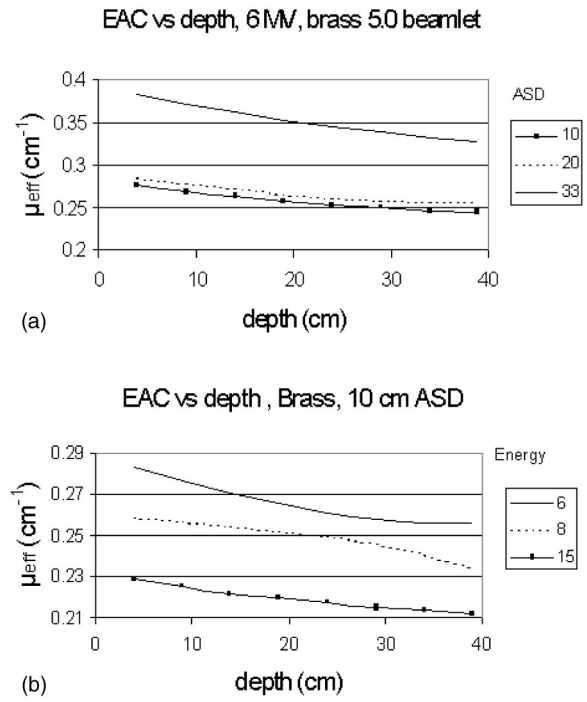

FIG. 8. The variation of the effective attenuation coefficient for brass as a function of depth for 10, 20, and 33 cm absorber-to-skin-distance (ASD) (a) and for 6, 8, and 15 MV beam energies at a ASD of 10 cm (b). In both cases a fixed square beamlet with a side length of 5 cm was used.

age error on the dose for an extreme case is given by the relation

$$|\delta\mu_{\text{eff}}| = \frac{1}{t}\ln\left(\frac{1+\sigma}{1-\sigma}\right), \tag{5}$$

where $\sigma = \delta D/D$.

The percentage difference between the fitted depth dose data and the raw DOSXYZ data was on average of the order of 0.3%. Substitution of $t = 1.0$ cm and $\sigma = 0.3$ into Eq. (5) yields, $|\delta\mu_{\text{eff}}| = 0.006\ \text{cm}^{-1}$. This corresponds to a percentage error of the order of 3% in the effective attenuation coefficient. At greater depths scatter effects lead to a further decrease in the effective attenuation coefficient values.

At this point a discussion of the effect of the voxel size on the accuracy of the results is in order. Tests have indicated that the depth dose data generated for a voxel size with the same lateral dimensions in the x and y directions, but reduced to 0.5 cm in the z direction gave absolute depth dose results that differ less than 1% compared to a similar simulation but with a voxel dimension of 1.0 cm in the z direction. These differences are related to the variance of the comparative depth dose data. The largest differences were found near the phantom (water) surface but our results are based on smoothed depth dose data for depths greater than 4 cm. It is therefore not expected that the smaller voxel size would lead to results that would influence the values of the effective attenuation coefficients appreciably.

In Fig. 6 the EAC vs depth is shown for various beam absorber materials. These curves decrease with depth in accordance with the observed results in Fig. 5. The same data is used to plot the EAC as a function of atomic number in Fig. 7. The higher EAC value of brass when compared with the fitting curve is a result of statistical variance. If an effective beam energy of 2 MeV is assumed then the linear attenuation coefficient for copper is $0.38\ \text{cm}^{-1}$ compared to $0.36\ \text{cm}^{-1}$ for brass. These values are of the same order as those shown in Fig. 7. For low-density materials such as wax and aluminum the dose variations with depth might become more important when a single value of the EAC with depth is assumed. The variation of the EAC with depth must then be taken into account. From Eq. (2) the percentage variation in dose could be expressed as

$$\frac{\text{Dose}_{\text{actual}}}{\text{Dose}_{\text{planned}}} = \exp(-\delta\mu_{\text{eff}}t), \tag{6}$$

where $\text{Dose}_{\text{actual}}$ is the actual dose and $\text{Dose}_{\text{planned}}$ is planned dose that one would have liked to have.

In this study all EAC data were derived for an absorber-to-skin-distance (ASD) of 33 cm (see Fig. 1). No extensive investigation into the variance of these coefficients with retracting distance was made. The variation of the EAC as a function of retracting distance is well known.[11,21] From Figs. 8(a) and 8(b) it can be seen that the values of the coefficients are less at short distances due to dose enhancement from scattered radiation from the beam absorbers that reaches the water phantom. This effect is less at larger distances since scattered radiation does not reach the central scoring region in the water phantom.

The EACs were derived on the central axis (CAX). The values of these coefficients would change radially from the CAX in a real beam, since there is a change in the spectral properties of the beam partly due to the shape of the flattening filter and the angular distribution of bremstrahlung pho-

TABLE V. Monte Carlo calculated EAC values, in units of (cm^{-1}), at 4 cm depth in water. For comparison, the data in parentheses for aluminum and wax were measured and the data for brass and lead were taken from the literature.

Energy (MV)	Wax	Aluminum	Brass	Lead
6	0.037 (0.040)	0.131 (0.11)	0.386 (341)	0.571 (0.58)[a]
8	0.034 (0.035)	0.115 (0.099)	0.350 (0.309)	0.537 (0.52)[a]
15	0.028 (0.028)	0.098 (0.085)	0.313 (0.290)	0.527 (0.51)[a,b]

[a]Reference 35.
[b]EAC value for 16 MV x rays.

tons emerging from the target.[30,31] Larson *et al.*[32] approximated the radial dependence of the effective attenuation coefficient for a lead filter with a linear function $\mu(r) = 0.0539 + 0.0005r(\mathrm{cm}^{-1})$ for a 4 MV beam. Bjärngard and Shackford[33] measured attenuation factors in water and found a quadratic dependence of the effective attenuation coefficient as a function of radius in water of the form $\mu(r) = 0.0473(1 + 0.000\,33r^2)$. This relationship was found for a 6 MV open beam generated by a Philips SL75-5 linac. Thomas and co-workers[34–36] measured the radial variation of beam quality for 8 MV x rays in water for a tungsten alloy filter. They found a linear relationship for the effective attenuation coefficient expressed as a function of the azimuthal angle ϕ, between the CAX and the radial position on the surface of the water phantom. Their equation for the effective attenuation coefficient was $\mu = 0.037 + 0.020\phi$. Apart from field size and to a lesser extent, depth dependencies, the EAC depend significantly on spectral changes introduced off-axis by flattening filters.

Others[16,17] have also incorporated an attenuator thickness, t, dependence in their EAC parametrization equations that is absent from ours [Eq. (4)], but used larger field sizes. Our study indicated an exponential decline in the absorbed dose as a function of absorber thickness over the field size range used. Larger fields from linacs would introduce radial spectral changes that enhance the dose and thus decrease the EAC. This could alter the simple exponential relationship found between dose and attenuator thickness [e.g., $T(x) = \exp(-\mu x)$, Eq. (2)] to an expression $T(x) = \exp(-\mu x(1 - \eta x))$: the type used by Bjärngard and Shackford.[33]

In Table V the measured EAC data differ from the Monte Carlo calculated data on average in the order of 10%. The reason for this is that the beam model used in DOSXYZ was a simple nondiverging x-ray beam where the energy spectra was uniform throughout the beam. The x-ray source spectra included many off-axis soft x-ray components not present in a real beam on the CAX. This could explain why the measured attenuation coefficients were lower in aluminum than in the MC simulations. Wax does not cause significant beam hardening and thus the difference in the measured and simulated EAC is not as large as in the case of aluminum and can be regarded as insignificant for 8 and 15 MV x rays. When these EAC's are used for compensator construction, care must be taken that the beamlet models must include scatter. Otherwise the broad beam attenuation coefficient must be used.

V. CONCLUSION

In this study EACs were derived for three different x-ray beam energies and a range of beamlet sizes. It was found for brass and aluminum that their EAC values decrease as a function of depth and x-ray beam energy, the dependence on the depth is much weaker than that of field size and can be conveniently parametrized. The EAC values vs Z could also be parametrized. The DOSXYZ calculated results show good correspondence with measured and other data. These EACs can also be used for compensator manufacturing since it takes beam hardening and the scatter properties of x rays in the beamlets directly into account and is based on absorbed dose values, rather than linear attenuation coefficients, which are based on the conversion of fluence to dose.

ACKNOWLEDGMENT

This work was supported by a grant from the Medical Research Council of South Africa.

[a]Current address: Medical Physics Department, Faculty of Medicine, University of the Free State, P.O. Box 339, Bloemfontein, 9300 South Africa.

[1] F. Ellis, A. Feldman, and R. Oliver, "A compensator for variations in tissue thickness for high energy beams," Br. J. Radiol. **32**, 421 (1959).
[2] F.M. Khan, V.C. Moore, and D.J. Burns, "The construction of compensators for cobalt teletherapy," Radiology **96**, 187–192 (1970).
[3] P.M.K. Leung, J. Van Dyk, and J. Robins, "A method of large irregular field compensation," Br. J. Radiol. **47**, 805–810 (1974).
[4] D.M. Robinson and J.W. Scrimger, "Optimized tissue compensators," Med. Phys. **17**, 391–396 (1990).
[5] E. El-Khatib, E.B. Podgorsak, and C. Pla, "Calculation of dose in homogeneous phantoms for partially attenuated photon beams," Med. Phys. **13**, 928–935 (1986).
[6] J.E. Marrs, A.R. Hounsell, and J.M. Wilkinson, "The efficacy of lead shielding in megavoltage radiotherapy," Br. J. Radiol. **66**, 140–144 (1993).
[7] E. El-Khatib, E.B. Podgorsak, and C. Pla, "Calculation of dose in homogeneous phantoms for partially attenuated photon beams," Med. Phys. **15**, 145–150 (1988).
[8] E. Papiez and G. Froese, "The calculation of transmission through a photon beam attenuator using sector integration," Med. Phys. **17**, 281–286 (1990).
[9] M.E. Castellanos and J.C. Rosenwald, "Evaluation of the scatter field for high-energy photon beam attenuators," Phys. Med. Biol. **43**, 277–290 (1998).
[10] S.J. Thomas and G. Bruce, "Skin dose near compensating filters in radiotherapy," Phys. Med. Biol. **33**, 703–710 (1988).
[11] P-H. Huang and B.E. Bjärngard, "Scattered photons produced by beam-modifying filters," Med. Phys. **13**, 57–63 (1986).
[12] J. Van Dyk, "Broad beam attenuation of cobalt-60 gamma rays and 6-, 18-, and 25-MV x rays by lead," Med. Phys. **13**, 105–110 (1986).
[13] A. Ahnesjö, L. Weber, and P. Nilsson, "Modeling transmission and scatter for photon beam attenuators," Med. Phys. **22**, 1711–1721 (1995).
[14] F.R. Bagne, N. Samsami, S.W. Hoke, and D.G. Bronn, "A study of effective attenuation coefficient for calculating tissue compensator thickness," Med. Phys. **17**, 117–121 (1990).
[15] E.C. McCullough, J. Gortney, and C.R. Blackwell, "A depth dependence determination of the wedge transmission factor for 4–10 MV photon beams," Med. Phys. **15**, 621–626 (1988).
[16] A.L. Boyer, "Compensating filters for high energy x rays," Med. Phys. **9**, 429–433 (1988).
[17] K.J. Weeks, B.A. Fraass, and K.M. Hutchins, "Gypsum mixtures for compensator construction," Med. Phys. **15**, 410–414 (1988).
[18] V.R. Arora and K.J. Weeks, "Characterization of gypsum attenuators for radiotherapy dose modification," Med. Phys. **21**, 77–81 (1994).
[19] C-M. Ma, P. Reckwerdt, M. Holmes, D.W.O. Rogers, and B. Geiser, *DOSXYZ Users Manual* (National Research Council of Canada, NRC, Ottowa, 1995).
[20] B.E. Bjärngard, J.-S. Tsai, and R.K. Rice, "Attenuation in very narrow photon beams," Radiat. Res. **118**, 195–200 (1989).
[21] W. Sewchand, N. Bautro, and R.M. Scott, "Basic data on tissue-equivalent compensators for 4-MV x-rays," Int. J. Radiat. Oncol., Biol., Phys. **6**, 327–332 (1980).
[22] K.P. Mandal, D.H. Baxter, and P. Ray, "Thin lead sheets as tissue compensators for larger field irradiation," Int. J. Radiat. Oncol., Biol., Phys. **6**, 513–517 (1980).
[23] A. Djordevich, D.J. Bonham, E.M.A. Hussein, J.W. Andrew, and M.E. Hale, "Optimal design of radiation compensators," Med. Phys. **17**, 397–404 (1990).
[24] J.S. Li, T. Pawlicki, J. Deng, S.B. Jiang, E. Mok, and C.-M. Ma, "Vali-

dation of a Monte Carlo dose calculation tool for radiotherapy treatment planning,'' Phys. Med. Biol. **45**, 2969–2985 (2000).
[25] S.X. Chang, T.J. Cullip, and K.M. Deschesne, ''Intensity modulation delivery techniques: 'Step & shoot' MLC auto-sequence versus the use of a modulator,'' Med. Phys. **27**, 948–959 (2000).
[26] W.R. Nelson, H. Hirayama, and D.W.O. Rogers, The EGS4 Code System SLAC-Report-265, Stanford Linear Accelerator Center, 1985.
[27] D.W.O. Rogers, B.A. Faddegon, G.X. Ding, C.-M. Ma, J. We, and T.R. Mackie, ''BEAM: A Monte Carlo code to simulate radiotherapy treatment units,'' Med. Phys. **22**, 503–525 (1995).
[28] C.-M. Ma and D.W.O. Rogers, BEAMDP Users Manual, National Research Council of Canada, Report No. PIRS-0509B (NRC, Ottawa, 1995).
[29] J.H. Hubbell and S.M. Seltzer, Tables of x-ray mass attenuation coefficients and mass energy-absorption coefficients 1 keV to 20 MeV for elements $Z=1$ to 92 and 48 additional substances of dosimetric interest, NISTIR 5632, 1995.
[30] W.H. Hanson and L.W. Berkley, ''Off-axis beam quality change in linear accelerator x-ray beams,'' Med. Phys. **7**, 145–146 (1980).
[31] R. Mohan, C. Chui, and L. Lidofsky, ''Energy and angular distributions from medical linear accelerators,'' Med. Phys. **12**, 592–597 (1985).
[32] R.D. Larsen, L.H. Brown, and B.E. Bjärngard, ''Calculations for beam-flattening filters for high-energy x-ray machines,'' Med. Phys. **5**, 215–220 (1978).
[33] B.E. Bjärngard and H. Shackford, ''Attenuation in high-energy x-ray beams,'' Med. Phys. **21**, 1069–1073 (1994).
[34] S.J. Thomas and R.L. Thomas, ''A beam generation algorithm for linear accelerators with independent collimators,'' Phys. Med. Biol. **35**, 325–332 (1990).
[35] S.J. Thomas, ''A computer-calculated tissue compensator system,'' Br. J. Radiol. **58**, 665–668 (1993).
[36] E.E. El-Khatib, E.B. Podgorsak, and C. Pla, ''The effect of lead attenuators on dose in homogenous phantoms,'' Med. Phys. **13**, 928–935 (1986).